Extraordinary Enhancement of Raman Scattering from Pyridine on Single Crystal Au and Pt Electrodes by Shell-Isolated Au Nanoparticles

Jian-Feng Li,[†,‡] Song-Yuan Ding,[†,§] Zhi-Lin Yang,[∥] Mei-Lin Bai,[⊥] Jason R. Anema,[†] Xiang Wang,[†] An Wang,[†] De-Yin Wu,[†] Bin Ren,[†] Shi-Min Hou,[⊥] Thomas Wandlowski,*[‡] and Zhong-Qun Tian*[†]

[†]State Key Laboratory of Physical Chemistry of Solid Surfaces and College of Chemistry and Chemical Engineering, Xiamen University, Xiamen, 361005, China

[‡]Department of Chemistry and Biochemistry, University of Bern, Freiestrasse 3, Bern CH-3012, Switzerland

[§]Theoretical Chemistry, VU Amsterdam, De Boelelaan 1083, HV Amsterdam 1081, The Netherlands

[∥]Department of Physics, Xiamen University, Xiamen, 361005, China

[⊥]Key Laboratory for Physics and Chemistry of Nanodevices and Department of Electronics, Peking University, Beijing, 100871, China

S *Supporting Information*

ABSTRACT: We used shell-isolated nanoparticle-enhanced Raman spectroscopy (SHINERS) to systematically study the adsorption of pyridine on low-index Au(hkl) and Pt(hkl) single crystal electrodes. Our gold-core silica-shell nanoparticles (Au@SiO$_2$ NPs) boost the intensity of Raman scattering from molecules adsorbed on atomically flat surfaces. The average enhancement factor reaches 10^6 for Au(110) and 10^5 for Pt(110), which is comparable to or even greater than that obtained for bare gold NPs (a widely adopted SERS substrate). 3D-FDTD simulations reveal that this large enhancement is due to the transfer of the "hotspots" from NP-NP gaps to NP-surface gaps. We also found that the SHINERS intensity strongly depends on the surface crystallographic orientation, with differences up to a factor of 30. Periodic DFT calculations and theoretical analysis of dielectric functions indicate that this facet-dependence is predominantly governed by the dielectric property of the surface. The results presented in this work may open up new approaches for the characterization of adsorbates and reaction pathways on a wide range of smooth surfaces.

Spectroscopy affords a powerful way to explore structure and reaction pathways at surfaces. Raman spectroscopy[1] in particular provides fingerprint information to fully characterize surface species. However, Raman scattering is intrinsically weak and at surfaces only a (sub)monolayer of molecules contribute the desired structural information. Signal strength may be increased by using surface plasmons (SPs)[2] to focus light; however this strategy requires nanoscale features to support localized or propagating SP modes, and therefore classical surface-enhanced Raman scattering (SERS)[3] is not applicable to the study of atomically flat single crystal surfaces. Thus, new structurally sensitive in situ techniques are necessary, as well-defined single crystals are an essential platform for exploring correlations between interfacial structure and reactivity in surface science.

Tip-enhanced Raman spectroscopy (TERS)[4] and attenuated total reflection (ATR)[5] are two methods of focusing light which have been used to increase signal strength in the study of single crystal surfaces. However, both approaches have their limitations.

With ATR, the number of molecules sampled is large but the enhancement factor (EF) is only 1 to 2 orders of magnitude. With TERS, the EF may be as high as 10 orders of magnitude,[6] but only a few molecules, which are located in the nanosized gap between tip and single crystal surface, are sampled. Consequently, the total number of Raman scattered photons is much smaller than that of SERS. The rather limited number of works employing both techniques including ordinary SERS to single crystal surface studies illustrates the severe difficulties in their practical implementation.[7] Alternative approaches are highly desirable to expand the morphological generality of SERS.

Recently, we have introduced shell-isolated nanoparticle-enhanced Raman spectroscopy (SHINERS).[8] Here, thousands of nanoparticles (NPs) with a gold core and an ultrathin silica shell are spread over a surface. The gold core focuses light and provides Raman signal enhancement by acting as a SP substrate while the silica shell prevents the core from interfering with the system under study. The great advantage of SHINERS is that it combines the strengths of ATR and TERS: many molecules benefit from the enhancement (as in ATR), and the EF is quite large (as in TERS). We and Gewirth's group have already shown that this method can be used to obtain high-quality spectra from atomically smooth Au(111), Au(100), Pt(111), Cu(111), Cu(100), and Rh(111) single crystal surfaces,[9] but the systematic exploration of other facets and the quantitative evaluation of Raman scattering enhancement remain as significant obstacles to the development of SHINERS as a general tool for surface science.

In the present work we report high-quality SHINERS spectra of pyridine adsorbed on low-index Au(hkl) and Pt(hkl) electrodes. We use three-dimensional finite-difference time-domain (3D-FDTD) simulations and slab-model based periodic density functional theory (DFT) calculations to address the nature of the unexpectedly strong Raman signal observed.

SHINERS NPs having a gold core ($\sim$55 nm in diameter) and an ultrathin silica shell (2−3 nm) were prepared according to refs 8 and 9c. Bare gold NPs ($\sim$55 nm in diameter) were synthesized according to the same method as the one used to prepare the SHINERS NP core and used for comparison. These shell-isolated
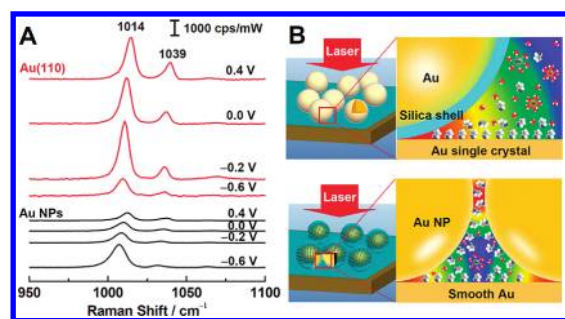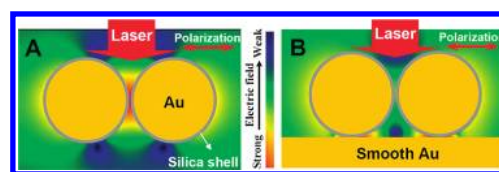
Figure 1. (A) SHINERS spectra of pyridine on Au(110) and SERS spectra of pyridine on bare 55 nm gold NPs at different potentials. Solution: 10 mM pyridine + 0.1 M $NaClO_4$. (B) Schematic diagrams of the SHINERS and SERS experiments. The EM field strength is represented by the following color code: red (strong) and blue (weak). For details of the FDTD simulations see Figure 2.


Figure 2. 3D-FDTD simulations showing EM field distribution in a plane through the interparticle axis for a SHINERS NP dimer in air (A), and the same dimer placed on a perfectly smooth gold surface (B). Direction of incidence and polarization of the 632.8 nm excitation laser are as shown. The diameter of the gold core is 55 nm, the thickness of the silica shell is 2 nm, and the distance between the NPs is 2 nm.

NPs or bare NPs were then deposited onto Au(hkl) or Pt(hkl) single crystal hemisphere bead electrodes[10] and subsequently mounted under potential control in a custom-made spectroelectrochemical cell[9a] (a Pt and a Ag/AgCl electrode served as counter and reference electrodes, respectively). Localized SP modes enhance electromagnetic (EM) field strength in NP-NP gaps and NP-surface gaps during irradiation with a HeNe laser ($\lambda = 633$ nm), and they boost the intensity of Raman scattering from molecules adsorbed nearby. Further experimental details are given in the Supporting Information (SI 1).

SHINERS spectra of pyridine on Au(110) and SERS spectra of pyridine on bare gold NPs were obtained for comparison under the same experimental conditions (see SI 2), and two striking features may be found in Figure 1A. First, SHINERS intensity from pyridine on Au(111) is comparable to or greater than the SERS intensity from pyridine on bare gold NPs (see SI 3). We estimated average experimental EFs of about 10^6 for SHINERS and 10^5 for SERS (see SI 4). This result is quite surprising because SP coupling between gold NPs has long been considered more efficient than the coupling between NPs and smooth surface. Second, we found that the potential-dependent intensity profiles were distinctly different for SHINERS and SERS (Figure 1A and SI Figure S1). The intensities of the vibrational bands at 1014 and 1039 cm^{-1}, which are characteristic for adsorbed pyridine[6] and depend strongly on the applied potential, reach a maximum at -0.20 V in the SHINERS experiment and at -0.60 V in the SERS experiment.

These two experiments are illustrated in Figure 1B. In SHINERS, pyridine is adsorbed only on the single crystal surface. The enhanced Raman scattering originates exclusively from pyridine molecules adsorbed on this surface since the pinhole-free (see SI 5) SHINERS NPs are chemically and electrically inert. In the SERS experiment, a smooth polycrystalline gold surface is used instead of a single crystal one because the NPs themselves are polycrystalline. Pyridine is adsorbed both on the bare gold NPs and on the smooth gold surface, but the EM field strength is maximized in the spaces between bare gold NPs (see SI 3) and therefore most of the signal arises from pyridine molecules located there. Consequently, bare gold NPs cannot provide enhanced Raman information from adsorbed species and/or surface reactions on well-defined single crystal surfaces. Our SHINERS method can resolve this problem and, therefore, has the potential to become a powerful tool in surface science and related areas.

The 3D-FDTD method[11] was used to simulate the EM field strength in the vicinity of shell-isolated gold NPs and bare gold NPs in order to better understand the nature of the strong Raman scattering from pyridine on Au(110) in our SHINERS experiments. Figure 2 shows that the placement of two SHINERS NPs (2 nm spacing between their silica shells) on a free-electron metal support leads to a very efficient transfer of the location of greatest EM field enhancement, the so-called "hotspot", from the NP-NP gap to the NP-surface gap. The theoretical EF for the hotspot in Figure 2B is calculated as 5×10^7.

Figure 2 also shows that the field distribution is not uniform. However, the intensity of an experimentally obtained Raman signal represents the sum of contributions from molecules located all over the substrate. Therefore, we also calculated an average SHINERS intensity by integrating over the entire area modeled, which includes regions of high (red), moderate (yellow-green), and weak (blue) enhancement. The average EF obtained in this way is about 4×10^5. This value is in agreement with our experimental observations if we assume a chemical EF of about 10.[12] The magnitude of the enhancement was unexpected because the incident light was polarized horizontally from NP center to NP center rather than vertically, and it has long been thought that the hotspot for all kinds of surface-immobilized NPs is located between the NPs. In fact, this unexpected transfer of the hotspot from the gap between NPs to the gap between NP and support provides a unique opportunity for the characterization of adsorbed species on a wide range of surfaces by efficient and selective enhancement of Raman scattering.

Comparative experiments of pyridine adsorbed on the three low-index unreconstructed Au(hkl)-(1×1) single crystal surfaces[13] show that SHINERS intensity is strongly dependent on the surface crystallographic orientation. Figure 3A illustrates the trend at a substrate potential of 0.00 V. The Raman signal from Au(110) is about eight times stronger than that obtained from Au(100) and about 30 times stronger than that obtained from Au(111). We note that the latter of these two values is much too large to be caused by a change in the orientation of adsorbed pyridine. Figure 3B further illustrates that this trend is rather independent of the applied electrode potential. Dielectric properties of the surface, such as the ones inherent in electroreflectance (ER), substrate—adsorbate coordination, and interactions of solvent molecules (water) with pyridine and the various gold surfaces, may contribute to the large intensity differences observed.

In an attempt to better understand this surface crystallographic orientation dependent Raman effect, we performed slab-model based DFT calculations using the Vienna *ab initio* simulation package (VASP).[14] In particular, we calculated the interaction energy E_{int}(Py-S) for pyridine and the surface, the zz component of the polarizability α of the clean and pyridine-modified
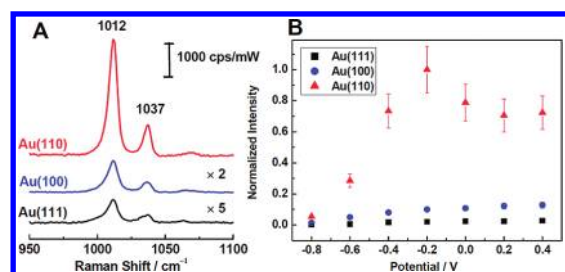
Figure 3. (A) SHINERS spectra of pyridine adsorbed on Au(111), Au(100), and Au(110) at 0.00 V. Solution: 10 mM pyridine + 0.1 M NaClO$_4$. (B) Normalized SHINERS intensities of the v_1 ring breathing mode of pyridine on Au(111), Au(100), and Au(110) at different potentials.

Table 1. Calculated Bond Length of N–Au, the Interaction Energies for Pyridine and the Surfaces, zz Component of the Polarizability α_{zz} for the Clean Surface (S) and for the Pyridine-Surface (Py-S) Complexes, and the Raman Scattering Factor S_1 for the v_1 Ring Breathing Mode

Py-Au(hkl)- (2 × 2)	B(N-Au)^a	E_{int} (Py-S)^b	α_{zz} (× 10^4) (S)^c	(Py-S)^c	S_1 (× 10^5)^d
Au(111)	2.592	16.1	2.626	3.264	1.8
Au(100)	2.440	27.6	2.641	3.360	5.0
Au(110) ^{e}	2.328	42.3	2.827	3.661	5.2
Au(110) ^{f}	2.342	41.9	2.827	3.673	6.9

^{a} Bond length in Å. ^{b} Interaction energy in kJ mol^{-1}. ^{c} Polarizability in Å^3. ^{d} Raman scattering factor in Å^4/amu. The definitions of footnotes $b-d$ are explained in SI 6. ^{e} The Py-Au(110) (2 × 2) configuration with the pyridine plane site along [001]. ^{f} The Py-Au(110) (2 × 2) configuration with the pyridine plane site along [1 $\bar{1}$0].

surface, and the Raman scattering factor for the v_1 ring breathing mode around 1012 cm^{-1} in the static limit. Table 1 shows that the interaction between pyridine and a gold surface increases in the order Au(111) < Au(100) < Au(110). This trend is consistent with the experimental Gibbs energies of pyridine adsorbed on the Au(hkl) surface using chronocoulometry.[13] In the same sequence, both the clean surface and the pyridine-modified surface become increasingly polarizable in the z direction and the Raman intensity of the v_1 mode gets stronger from Au(111) to Au(110) (computational details are given in SI 6). We note that this first principle simulation of the pyridine-Au(hkl) system reproduces the trend in, but not the magnitudes of, the experimentally observed Raman intensities of the v_1 mode. Clearly, then, the high intensities seen in the SHINERS data in Figure 1A and Figure 3 are not dominated by contributions from chemisorption of the adsorbate.

Next we explore the role of the polarizability α. The microscopic *quantity* α is connected with the macroscopic quantity dielectric constant, ε, through the approximated Clausius–Mossotti relation[15] $(\varepsilon - \varepsilon_m)/(\varepsilon + 2\varepsilon_m) = 4\pi\alpha/3V$ (where ε_m is the dielectric constant of the surrounding medium and V is the volume of the cell). Different *polarizabilities* α_{zz} of the clean and pyridine-modified Au(hkl) surfaces, as obtained in the DFT calculations (although they are static ones), may reflect different dielectric constants of the three low-index gold electrodes. Furthermore, these different dielectric constants may lead to distinct EM coupling between our SHINERS NPs and the different crystallographic orientation. The facet-dependent
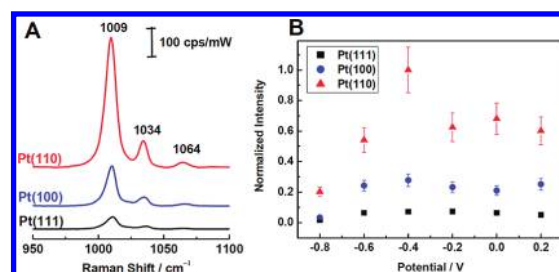
Figure 4. (A) SHINERS spectra of pyridine adsorbed on Pt(111), Pt(100), and Pt(110) at 0.00 V. Solution: 10 mM pyridine + 0.1 M NaClO$_4$. (B) Normalized SHINERS intensity for the v_1 ring breathing mode of pyridine on Pt(111), Pt(100), and Pt(110) at different potentials. The indicated standard deviation represents the scatter from measurements at different spots as well as different samples.

dielectric properties can be correlated with optical transitions involving surface states; then the dielectric constants can in principle be extracted from experimental ER spectra.[16] Liu et al. reported that the absorption energy of Au(110) in aqueous HClO$_4$ or NaF electrolyte is in a broad potential range much larger (above 3 eV) than that of Au(111) and Au(100) under identical experimental conditions.[17] This trend reveals that the imaginary part of the dielectric function, ε_{im}, for Au(110) should be much smaller than ε_{im} for Au(111) and Au(100) when illuminated with a red laser (632.8 nm in wavelength, 1.96 eV in energy).[18] A detailed theoretical analysis of the correlation between dielectric constants and excitation energies is given in SI 7. Furthermore, the Clausius–Mossotti relation predicts that the imaginary part of the dielectric constant of a metal, ε_{im}, dominates the enhanced EM field if the resonant condition $|\varepsilon_{re} + 2\varepsilon_m| \approx 0$ (also known as the Fröhlich condition) is fulfilled.[15] Therefore, the higher Raman intensity on the Au(110) system can be attributed to a much stronger EM field originating from the smaller value of ε_{im}. This smaller value of ε_{im} means less absorption at 1.96 eV and translates into a higher ER for the Au(110) surface. We conclude that the facet-dependent SHINERS intensity reported here for pyridine on low-index Au(hkl)-(1 × 1) surfaces is most probably dominated by the dielectric properties of the interface.

In an attempt to generalize our observations with pyridine on Au(hkl), we also carried out preliminary experiments with Pt(hkl) electrodes, a nontraditional SERS substrate. The data plotted in Figure 4A present the first high-quality Raman spectra on the three low-index facets of platinum single crystals under electrochemical conditions. The average EF for Pt(110) is about 10^5, which is as high as the one obtained for bare gold NPs on smooth gold (see SI 4). We also note that this value is significantly higher than the EF obtained for electrochemically roughened platinum electrodes (EF ≈ 10^2) or gold-core platinum-shell NPs (EF ≈ 10^4).[6] Figure 4B shows the potential dependence of the normalized SHINERS intensity for pyridine on Pt(111), Pt(100), and Pt(110). Low-index Pt(hkl) surfaces show the same qualitative trend in SHINERS intensity as Au(hkl) ones do, except that a common maximum occurs at about −0.4 V. The SHINERS intensity for Pt(110) is about three times stronger as compared to Pt(100) and about ten times stronger than that for Pt(111). We also note that the dependence of the intensity for Pt(hkl) on the crystallographic orientation is not as significant as that for Au(hkl). This is probably related to dielectric properties and the resulting smaller ER for platinum electrodes, and it supports the explanation we proposed for Au(hkl).

In summary, the proposed SHINERS approach shows strong Raman signals from pyridine adsorbed on atomically flat, low-index Au(hkl) and Pt(hkl) single crystal electrodes. The average EF reaches 10^6 for Au(110) and 10^5 for Pt(110), which is comparable to or even higher than what is obtained for bare gold NPs on smooth gold (a widely adopted SERS substrate). The experimental trends are confirmed by 3D-FDTD theoretical simulations.

Based on our DFT calculations and theoretical analysis, we conclude that the SHINERS intensities observed for pyridine on Au(hkl) and Pt(hkl) are dominated by dielectric properties of the single crystal surfaces, which leads to a considerably stronger EM field coupling between our SHINERS NPs and the (110) surface compared to other low-index surfaces. This facet-dependent Raman effect should, in principle, also be observed for the high-index single crystal surfaces; this will be the subject of future work in our lab.

The present paper illustrates the importance of combining *ab initio* polarizability calculations for the clean and adsorbate-modified electrodes with 3D-FDTD simulations of EM field distribution. Extending this work to include the effect of solvent molecules (and other components of the electrolyte), as well as an applied electric field, may offer exciting opportunities to represent the experimental system more realistically. The experimental discoveries reported in this communication open up unique approaches for the characterization of adsorption and reaction pathways on a wide range of smooth and well-characterized surfaces, such as single crystal metal and semiconductor electrodes, which were previously inaccessible due to severe signal-intensity limitations. Our SHINERS strategy may also be applicable to other surface spectroscopies, such as infrared absorption or sum frequency generation. SHINERS has tremendous potential for use as a versatile molecular vibration spectroscopy to study structurally well-defined surfaces of diverse materials widely used in surface science, electrochemistry, heterogeneous catalysis, self-assembly, adhesives, and semiconductor device fabrication.

■ ASSOCIATED CONTENT

ⓢ Supporting Information. Experimental details, Raman spectra of pyridine on Au(110) and bare gold NPs, EF calculations, and computational details are presented in the Supporting Information (SI). This information is available free of charge via the Internet at http://pubs.acs.org.

■ AUTHOR INFORMATION

Corresponding Author
zqtian@xmu.edu.cn; thomas.wandlowski@dcb.unibe.ch

■ ACKNOWLEDGMENT

■ REFERENCES

(1) Long, D. A. *The Raman Effect: A Unified Treatment of the Theory of Raman Scattering by Molecules*; John Wiley & Sons Ltd.: Chichester, 2002.

(2) (a) Raether, H. *Surface Plasmons on Smooth and Rough Surfaces and on Gratings*; Springer-Verlag: Berlin, 1988. (b) Moskovits, M. *J. Raman. Spectrosc.* **2005**, *36*, 485–496. (c) Willets, K. A.; Van Duyne, R. P. *Annu. Rev. Phys. Chem.* **2007**, *58*, 267–297. (d) Le, F.; Lwin, N. Z.; Halas, N. J.; Nordlander, P. *Phys. Rev. B* **2007**, *76*, 165410.

(3) (a) Le Ru, E. C.; Etchegoin, P. G. *Principles of Surface-Enhanced Raman Spectroscopy and Related Plasmonic Effects*; Elsevier: Amsterdam, 2009. (b) Kneipp, K., Moskovits, M., Kneipp, H., Eds. *Topics in Applied Physics: Vol. 103, Surface-Enhanced Raman Scattering Physics and Applications*; Springer-Verlag: Berlin, 2006. (c) Aroca, R. *Surface-Enhanced Vibrational Spectroscopy*; John Wiley & Sons Ltd.: Chichester, 2006. (d) Faulds, K.; Smith, W. E.; Graham, D. *Anal. Chem.* **2004**, *76*, 412–417. (e) Baumberg, J. J.; Kelf, T. A.; Sugawara, Y.; Cintra, S.; Abdelsalam, M. E.; Bartlett, P. N.; Russell, A. E. *Nano Lett.* **2005**, *5*, 2262–2267.

(4) Deckert V. *J. Raman Spectrosc.* (Special issue) **2009**, *40* (10).

(5) (a) Bruckbauer, A.; Otto, A. *J. Raman. Spectrosc.* **1998**, *29*, 665–672. (b) Kretschmann, E.; Raether, H. Z. *Naturforschung* **1968**, *23A*, 2135–2136. (c) Futamata, M. *Surf. Sci.* **1997**, *386*, 89–92. (d) Chen, Y. X; Otto, A. *J. Raman. Spectrosc.* **2005**, *36*, 736–747.

(6) (a) Tian, Z. Q.; Ren, B.; Li, J. F.; Yang, Z. L. *Chem. Commun.* **2007**, 3514–3534. (b) Wu, D. Y.; Li, J. F.; Ren, B.; Tian, Z. Q. *Chem. Soc. Rev.* **2008**, *37*, 1025–1041.

(7) (a) Campion, A.; Mullins, D. R. *Chem. Phys. Lett.* **1983**, *94*, 576–579. (b) Mullins, D. R.; Campion, A. *Chem. Phys. Lett.* **1984**, *110*, 565–570. (c) Ikeda, K.; Fujimoto, N.; Uehara, H.; Uosaki, K. *Chem. Phys. Lett.* **2008**, *460*, 205–208. (d) Zheng, J. W.; Zhou, Y. G.; Li, X. W.; J, Y.; Lu, T. H.; Gu, R. A. *Langmuir* **2003**, *19*, 632–636. (e) Ikeda, K.; Suzuki, Shuto.; Uosaki, K. *Nano Lett.* **2011**, *11*, 1716–1722. (f) Brolo, A. G.; Irish, D. E.; Lipkowski, J. *J. Phys. Chem. B* **1997**, *101*, 3906–3909.

(8) (a) Li, J. F.; Huang, Y. F.; Ding, Y.; Yang, Z. L.; Li, S. B.; Zhou, X. S.; Fan, F. R.; Zhang, W.; Zhou, Z. Y.; Wu, D. Y.; Ren, B.; Wang, Z. L.; Tian, Z. Q. *Nature* **2010**, *464*, 392–395. (b) Anema, J. R.; Li, J. F.; Yang, Z. L.; Ren, B.; Tian, Z. Q. *Annu. Rev. Anal. Chem.* **2011**, *4*, 129–150.

(9) (a) Liu, B.; Blaszczyk, A.; Mayor, M.; Wandlowski, T. *ACS Nano* **2011**, *5*, 5662–5672. (b) Li, J. F.; Li, S. B.; Anema, J. R.; Yang, Z. L.; Huang, Y. F.; Ding, Y.; Wu, Y. F.; Zhou, X. S.; Wu, D. Y.; Ren, B.; Wang, Z. L.; Tian, Z. Q. *Appl. Spectrosc.* **2011**, *65*, 620–626. (c) Honestry, N. R.; Gewirth, A. A. *J. Raman. Spectrosc.* **2011**, DOI: 10.1002/jrs.2989.

(10) Clavilier, J.; Armand, D.; Sun, S. G.; Petit, M. *J. Electroanal. Chem.* **1986**, *205*, 267–277.

(11) (a) Kunz, K. S.; Luebbers, R. J. *The finite difference time domain method for electromagnetics*; CRC Press: LLC, Boca Raton, FL, 1993. (b) Sherry, L. J.; Chang, S. H.; Schatz, G. C.; Van Duyne, R. P. *Nano Lett.* **2005**, *5*, 2034–2038.

(12) (a) Zhao, L. L.; Jensen, L.; Schatz, G. C. *J. Am. Chem. Soc.* **2006**, *128*, 2911–2919. (b) Otto, A.; Mrozek, I.; Grabhorn, H.; Akemann, W. *J. Phys.: Condens. Matter* **1992**, *4*, 1143–1212.

(13) (a) Stolberg, L.; Lipkowski, J.; Irish, D. E. *J. Electroanal. Chem.* **1987**, *238*, 333–353. (b) Stolberg, L.; Lipkowski, J.; Irish, D. E. *J. Electroanal. Chem.* **1990**, *296*, 171–189. (c) Stolberg, L.; Morin, S.; Lipkowski, J.; Irish, D. E. *J. Electroanal. Chem.* **1991**, *307*, 241–262. (d) Lipkowski, J.; Stolberg, L.; Yang, D. F.; Pettinger, B.; Mirwald, S.; Henglein, F.; Kolb, D. M. *Electrochim. Acta* **1994**, *39*, 1045–1056.

(14) (a) Kresse, G.; Furthmüller *J. Comput. Mater. Sci.* **1996**, *6*, 15–50. (b) Kim, S.; Wang, Z.; Scherson, D. A. *J. Phys. Chem. B* **1997**, *101*, 2735–2740.

(15) Born, M.; Wolf, E. *Principle of Optics*, 7th ed.; Cambridge University Press: Cambridge, 1999.

(16) (a) Kolb, D. M.; McIntyre, J. D. E. *Surf. Sci.* **1971**, *28*, 321–334. (b) McIntyre, J. D. E. *Surf. Sci.* **1973**, *37*, 658–682. (c) Tadjeddine, A.; Kolb, D. M.; Kotz, R. *Surf. Sci.* **1980**, *101*, 277–285.

(17) Liu, S. H.; Hinnen, C.; Nguyen Van Huong, C.; de Tacconi, N. R.; Ho, K. M. *J. Electroanal. Chem.* **1984**, *176*, 325–338.

(18) Bohren, C. F.; Huffman, D. R. Classical Theories of Optical Constants. In *Absorption and Scattering of Light by Small Particles*; Wiley-VCH: Verlag GmbH, 2007; pp 226–267.